Line Enhancement and Completion via Linear Left Invariant Scale Spaces on $SE(2)$

Remco Duits[1,2] and Erik Franken[2]

[1] Dept. of Mathematics and Computer Science
[2] Dept. of Biomedical Engineering,
Eindhoven University of Technology, Den Dolech 2, P.O.Box 513,
5600 MB Eindhoven, The Netherlands
R.Duits@tue.nl, E.M.Franken@tue.nl

Abstract. From an image we construct an invertible orientation score, which provides an overview of local orientations in an image. This orientation score is a function on the group $SE(2)$ of both positions and orientations. It allows us to diffuse along multiple local line segments in an image. The transformation from image to orientation score amounts to convolutions with an oriented kernel rotated at multiple angles. Under conditions on the oriented kernel the transform between image and orientation score is unitary. This allows us to relate operators on images to operators on orientation scores in a robust way such that we can deal with crossing lines and orientation uncertainty. To obtain reasonable Euclidean invariant image processing the operator on the orientation score must be both left invariant and non-linear. Therefore we consider non-linear operators on orientation scores which amount to direct products of *linear* left-invariant scale spaces on $SE(2)$. These linear left-invariant scale spaces correspond to well-known stochastic processes on $SE(2)$ for line completion and line enhancement and are given by group convolution with the corresponding Green's functions. We provide the *exact* Green's functions and approximations, which we use together with invertible orientation scores for automatic line enhancement and completion.

1 Introduction

In many medical imaging applications elongated structures (such as catheters, blood-vessels and collagen fibres) appear only partially and vaguely in noisy medical image data, [9]. It is often desirable to process these images such that crossing elongated structures become more visible before actual detection takes place. Due to occlusions small parts of these line or edge-like structures may not be clearly visible, requiring line-completion, [15, 19, 1, 18, 7]. Furthermore, since the acquisition of, for example, X-ray images is harmful to a patient, the radiation dose is reduced as much as possible leading to very noisy images. Such images typically require *line-enhancement*, [9, 3] where the aim is to make the elongated structures more visible while reducing the noise.

In this article we will consider operators for line enhancement, using diffusion equations on the non-commutative group $SE(2)$ of planar translations

X.-C. Tai et al. (Eds.): SSVM 2009, LNCS 5567, pp. 795–807, 2009.

and rotations. This group $SE(2)$ is a semi-direct product of $\mathbb{R}^2$ and the circle $\mathbb{T} = \{e^{i\theta} \mid \theta \in [0, 2\pi)\} \equiv SO(2)$ and is equipped with the following product

$$gg' = (\mathbf{x}, e^{i\theta})(\mathbf{x}', e^{i\theta'}) = (\mathbf{x} + R_\theta \mathbf{x}', e^{i(\theta+\theta')}), \quad g = (\mathbf{x}, e^{i\theta}), g' = (\mathbf{x}', e^{i\theta'}) \in SE(2),$$

with $\mathbf{x} = (x, y) \in \mathbb{R}^2$ and $R_\theta = \begin{pmatrix} \cos\theta & -\sin\theta \\ \sin\theta & \cos\theta \end{pmatrix} \in SO(2)$.

Before we can apply line completion and enhancement to images we need a map $U_f : SE(2) \to \mathbb{C}$ which provides an overview of all local orientations in the image $f : \mathbb{R}^2 \to \mathbb{R}$. There exist several approaches to construct such a map, see for example [11], [4], [19], [1], but only few methods put emphasis on the stability of the inverse transformation $U_f \mapsto f$. However, well-posed image enhancement on the basis of local orientations in an image f can be done via the map U_f iff there exists a stable transformation between image f and map U_f.

In this article we restrict ourselves to the case where $U_f = \mathcal{W}_\psi f$ is given by

$$\mathcal{W}_\psi f(g) = \int_{\mathbb{R}^2} \overline{\psi(R_\theta^{-1}(\mathbf{y} - \mathbf{x}))} f(\mathbf{y}) \, \mathrm{d}\mathbf{y}, \quad g = (\mathbf{x}, e^{i\theta}) \in SE(2), R_\theta \in \mathrm{SO}(2), \quad (1)$$

i.e. the orientation score $\mathcal{W}_\psi f$ is obtained from image f by convolution with a directed anisotropic kernel $\psi \in \mathbb{L}_2(\mathbb{R}^2)$ rotated at multiple angles. In section 2 we will show that for a certain class of directional kernels ψ, we obtain quadratic norm preservation and thereby a stable reconstruction formula. This allows us to relate operators on images to operators on orientation scores via a robust commuting diagram, see Figure 1 (where the precise details will follow later).

Note that an invertible orientation score has useful properties: It carries per position a whole distribution of orientations and by invertibility it automatically unwraps crossing lines, [9, 8]. So instead of applying a diffusion directly on the image f we apply anisotropic diffusion on the corresponding orientation score $\mathcal{W}_\psi f$ such that we take advantage of these properties. Now in order to obtain Euclidean invariant smoothing of the image the diffusion on the orientation score must be left invariant and therefore in section 3 we consider left invariant diffusions on orientation scores. These diffusions are Fokker-Plank PDE's of well-known stochastic processes for line completion and enhancement. We provide their exact solutions as $SE(2)$-convolutions with the explicit Green's functions, which were strongly required by Mumford [15], Citti [3] and many others [19], [1] but hitherto unknown. Since our exact derivation of the Green's functions (which are scale space kernels on $SE(2)$) is rather technical we omit the derivations here and focus only on the results. For details see our recent works [7], [6]. Instead we will consider the highly simplified case of scale space kernels on the circle $\mathbb{T}$, which is often used in image analysis and quite analogous to the $SE(2)$ case. This helps the reader to get a better grasp on the scale space kernels on $SE(2)$. Finally, we include an experiment for both line enhancement and line completion. Here the advantage of our approach compared to our previous work [8] on *non*-linear diffusion on $SE(2)$, is that it involves less parameters, it is easier to grasp from a stochastic point of view and easier to implement (in parallel). The drawback, however, is that this scheme is less adaptive. For various biomedical engineering applications we refer to our thesis, [9, 18, 4].

2 Invertible Orientation Scores

The transformation between an image $f : \mathbb{R}^2 \to \mathbb{R}$ and an orientation score $\mathcal{W}_\psi f : \mathbb{R}^2 \rtimes \mathbb{T} \to \mathbb{R}$ given by (1) is a wavelet transformation generated by a reducible representation $\mathcal{U} : SE(2) \to \mathcal{B}(\mathbb{L}_2(\mathbb{R}^2))$ of the Euclidean motion group $SE(2) = \mathbb{R}^2 \rtimes \mathbb{T}$ into the space of bounded operators in $\mathbb{L}_2(\mathbb{R}^2)$.

This important observation needs some explanation. By definition a representation of the group $SE(2)$ (with unit element $e = (\mathbf{0}, e^{i0})$) is an isomorphism between $SE(2)$ and the space of bounded operators on $\mathbb{L}_2(\mathbb{R}^2)$, which means that $\mathcal{U}_g \circ \mathcal{U}_h = \mathcal{U}_{gh}$ for all $g, h \in SE(2)$ and $\mathcal{U}_e = I$. In our case we have

$$\mathcal{U}_g f(\mathbf{y}) = f(R_\theta^{-1}(\mathbf{y} - \mathbf{x})), \quad \text{for all } f \in \mathbb{L}_2(\mathbb{R}^2), g = (\mathbf{x}, e^{i\theta}).$$

The transform which maps an image f to orientation score $\mathcal{W}_\psi f$ given by (1) can now be rewritten in an $\mathbb{L}_2$-inner product form:

$$\mathcal{W}_\psi[f](g) = (\mathcal{U}_g \psi, f)_{\mathbb{L}_2(\mathbb{R}^2)}, \quad g \in SE(2), \tag{2}$$

which is the standard group theoretical structure of a continuous wavelet transform. However, we restrict ourselves *initially* to a single scale, like in [11]. The issue of scale comes into play later on by the diffusions on the orientation scores. Note that in standard continuous wavelet theory on the group of translations, rotations and scalings, it is *not possible* to obtain a stable reconstruction from a single scale layer as this conflicts [6, ch:2] the admissibility condition, [12]. The same holds for edgelets, curvelets, ridgelets [2]. Moreover, the admissibility condition in standard wavelet theory, [12], requires the wavelet to oscillate in radial direction which is undesirable with the diffusions we consider later on.

However, in contrast to the standard approach, [12], our representation $\mathcal{U}$ is reducible, which means that there exists a closed subspace of $\mathbb{L}_2(\mathbb{R}^2)$ which is invariant under $\mathcal{U}_g$ for all $g \in SE(2)$. Consider for example the closed subspace:

$$\mathbb{L}_2^\varrho(\mathbb{R}^2) = \{f \in \mathbb{L}_2(\mathbb{R}^2) \mid \text{support}\{\mathcal{F}f\} \subset B_{\mathbf{0},\varrho}\}, \tag{3}$$

where $B_{\mathbf{0},\varrho}$ denotes a ball around $\mathbf{0} \in \mathbb{R}^2$ with radius $\varrho > 0$ and where fourier transform $\mathcal{F} : \mathbb{L}_2(\mathbb{R}^2) \to \mathbb{L}_2(\mathbb{R}^2)$ is given by $\mathcal{F}f(\boldsymbol{\omega}) = \frac{1}{2\pi} \int_{\mathbb{R}} e^{-i\boldsymbol{\omega}\cdot\mathbf{x}} f(\mathbf{x}) \mathrm{d}\mathbf{x}$. Consequently, the celebrated result of Grossmann et al. [10] on stable reconstruction does not apply. Therefore in previous work [4] we showed that under minor conditions on ψ the wavelet transform $\mathcal{W}_\psi$ is a unitary map from $\mathbb{L}_2(\mathbb{R}^2)$ onto some reproducing kernel space of $\mathbb{L}_2$-functions on $SE(2)$. Here we avoid technicalities and just provide the essential formula which describes the stability:

$$\begin{aligned} &\int_{\mathbb{R}^2} \int_{\mathbb{T}} |(\mathcal{F}\mathcal{W}_\psi f)(\boldsymbol{\omega}, e^{i\theta})|^2 \mathrm{d}\theta \, \tfrac{1}{M_\psi(\boldsymbol{\omega})} \, \mathrm{d}\boldsymbol{\omega} = \int_{\mathbb{R}^2} \int_{\mathbb{T}} |(\mathcal{F}f)(\boldsymbol{\omega})|^2 |\mathcal{F}\psi(R_\theta^T \boldsymbol{\omega})|^2 \mathrm{d}\theta \, \tfrac{1}{M_\psi(\boldsymbol{\omega})} \, \mathrm{d}\boldsymbol{\omega} \\ &\quad = \int_{\mathbb{R}^2} |(\mathcal{F}f)(\boldsymbol{\omega})|^2 \mathrm{d}\boldsymbol{\omega} = \|f\|^2_{\mathbb{L}_2(\mathbb{R}^2)}, \end{aligned} \tag{4}$$

where $M_\psi \in C(\mathbb{R}^2, \mathbb{R})$ is *defined* by $M_\psi(\boldsymbol{\omega}) := \int_0^{2\pi} |\mathcal{F}\psi(R_\theta^T \boldsymbol{\omega})|^2 \mathrm{d}\theta$.

If ψ is chosen such that $M_\psi = 1$ then we get $\mathbb{L}_2$-norm preservation. However, this is not possible as $\psi \in \mathbb{L}_2 \cap \mathbb{L}_1(\mathbb{R}^2)$ implies that M_ψ is a continuous function

vanishing at infinity. This can be taken into account using distributional kernels [4]. In practice however, because of finite grid sampling, we can just restrict $\mathcal{W}_\psi$ to the space of bandlimited images $\mathbb{L}_2^\varrho(\mathbb{R}^2)$ given by (3) and use localized wavelets ψ with the property that $M_\psi(\omega) = \mathcal{M}(\rho)$, $\rho = \|\boldsymbol{\omega}\|$, where $\mathcal{M} : [0, \varrho] \to \mathbb{R}^+$ is a smooth approximation of $1_{[0,\varrho)}$. We call these wavelets proper wavelets. Exact reconstruction is obtained by the adjoint wavelet transform $\mathcal{W}_\psi^*$:

$$f = \mathcal{W}_\psi^* \mathcal{W}_\psi[f] = \mathcal{F}^{-1}\left[\boldsymbol{\omega} \mapsto \int_0^{2\pi} \mathcal{F}[U_f(\cdot, e^{i\theta})](\boldsymbol{\omega})\, \mathcal{F}[\mathcal{R}_{e^{i\theta}}\psi](\boldsymbol{\omega})\, \mathrm{d}\theta\, M_\psi^{-1}(\boldsymbol{\omega})\right], \quad (5)$$

where the rotated kernel is given by $\mathcal{R}_{e^{i\theta}}\psi(\mathbf{x}) = \psi(R_\theta^{-1}\mathbf{x})$. Now for proper wavelets one may as well use the (approximative) reconstruction:

$$\mathcal{F}^{-1}\left[\boldsymbol{\omega} \mapsto \int_0^{2\pi} \mathcal{F}[U_f(\cdot, e^{i\theta})](\boldsymbol{\omega})\, \mathcal{F}[\mathcal{R}_{e^{i\theta}}\psi](\boldsymbol{\omega})\, \mathrm{d}\theta\right] \quad (6)$$

In [4] we construct two different classes of proper wavelets. Here we shall briefly mention a typical example of one particular class (for the other class see [18, 4]) that even allows a reconstruction by integration over θ only, which is practical, fast and intuitive.

Example. Let B^k be a k-th order B-spline, i.e. $B^k = B^{k-1} * B^0$, with $B^0(x) = 1_{[-\frac{1}{2},\frac{1}{2}]}$ then we set (with $\boldsymbol{\omega} = (\rho\cos\phi, \rho\sin\phi)$):

$$\psi(\mathbf{x}) = \mathcal{F}^{-1}[\boldsymbol{\omega} \mapsto B^k\left(\frac{n_\theta(\phi \bmod 2\pi - \frac{\pi}{2})}{2\pi}\right)\mathcal{M}(\rho)](\mathbf{x}) \ ,$$

and where n_θ equals the number orientation samples in our orientation score, controls "kernel-width" and $\mathcal{M}(\rho) = e^{-\frac{\rho^2}{2\sigma^2}}(\sum_{k=0}^4 (-1)^k \left(2^{-1}\sigma^{-2}\rho^2\right)^k)^{-1}$, $\sigma = \frac{\varrho}{2}$.

Now that we have constructed a stable transformation between images f and corresponding orientation scores U_f we can relate operators Υ on images to operators Φ on orientation scores in a robust manner, see Figure 1. This relation is 1-to 1 if we ensure that the operator on the orientation score again provides an orientation score of an image. However the operators Φ that we will propose in the remainder of this article will not leave the space of orientations scores (which we from now on denote by $\mathbb{C}_K^{SE(2)}$) invariant, i.e. the processed orientation score will not be the orientation score of an image but just some enhanced square integrable element $\Phi(\mathcal{W}_\psi f)$ in $\mathbb{L}_2(SE(2))$. In practice however, this does not matter since we naturally extend the reconstruction formula to $\mathbb{L}_2(SE(2))$:

$$(\mathcal{W}_\psi^*)^{ext} U(g) = \mathcal{F}^{-1}\left[\boldsymbol{\omega} \mapsto \int_0^{2\pi} \mathcal{F}[U(\cdot, e^{i\theta})](\boldsymbol{\omega})\, \mathcal{F}[\mathcal{R}_{e^{i\theta}}\psi](\boldsymbol{\omega})\, \mathrm{d}\theta\, M_\psi^{-1}(\boldsymbol{\omega})\right](\mathbf{x}), \quad (7)$$

for all $U \in \mathbb{L}_2(SE(2))$, where $g = (\mathbf{x}, e^{i\theta}) \in SE(2)$. So there arise no practical problems, however one should be aware that the effective part of an operator Φ on an orientation score is in fact $\mathbb{P}_\psi \Phi$ where $\mathbb{P}_\psi = \mathcal{W}_\psi (\mathcal{W}_\psi^*)^{ext}$ is the orthogonal projection of $\mathbb{L}_2(SE(2))$ onto the space of orientation scores $\mathbb{C}_K^{SE(2)}$.

Next we give a brief motivation why *we must restrict ourselves to left invariant operators* on orientation scores: It can be verified that $\mathcal{W}_\psi \circ \mathcal{U}_g = \mathcal{L}_g \circ \mathcal{W}_\psi$ for all $g \in SE(2)$, where the left-regular representation $\mathcal{L} : G \to \mathcal{B}(\mathbb{L}_2(SE(2)))$ is

given by $\mathcal{L}_g U(h) = U(g^{-1}h)$. Consequently, the effective operator Υ on images is Euclidean invariant iff the operator Φ on orientation scores is left-invariant:

$$\Upsilon \circ \mathcal{U}_g = \mathcal{U}_g \circ \Upsilon \text{ for all } g \in SE(2) \;\Leftrightarrow\; \Phi \circ \mathcal{L}_g = \mathcal{L}_g \circ \Phi \text{ for all } g \in SE(2), \quad (8)$$

for further details see [4, Thm. 21, p.153]. It is well-known that the only left-invariant kernel operators are convolutions. On $SE(2)$ they are given by

$$(K *_{SE(2)} U)(g) = \int_{SE(2)} K(h^{-1}g)U(h)\,\mathrm{d}\mu(h) = \int_{\mathbb{R}^2}\int_0^{2\pi} K(R_{\theta'}^T(\mathbf{x}\text{–}\mathbf{x}'), \theta\text{–}\theta')\,U(\mathbf{x}', \theta')\mathrm{d}\theta'\mathrm{d}\mathbf{x}', \quad (9)$$

with $g = (\mathbf{x}, e^{i\theta})$ and μ the left-invariant Haar-measure on $SE(2)$. For a detailed overview of alternative algorithms (including complexity, steerability, performance, relation to Fourier transform on $SE(2)$, relation to tensor voting methods [9], [13] and extension to 3D), see the most complete and recent work [9, ch:3, p.53, p.72], containing new faster algorithms for steerable $SE(2)$ convolutions, [9, ch: 3.5.1], [18, ch: 6.5.1, 6.5.2], [4, ch: 7.8, 5.4, 5.3.2].

However, the operators on orientation scores should not be linear, since this would imply that the effective operator Υ is a rotation and translation invariant kernel operator and thereby [16], Υ would be a $\mathbb{R}^2$-convolution with an isotropic kernel. Clearly, in this case one does not require invertible orientation scores. Therefore, based on the works [19], [1], [17] on "completion fields", we consider so-called "collision distribution operators" which are given by

$$(\tilde{\Phi}(U, V))(g) = (R_\gamma *_{SE(2)} (\chi(U)))(g) \cdot (R_\gamma *_{SE(2)} (\chi(V)))(g), \quad (10)$$

where $R_\gamma(g) = \gamma \int_0^\infty e^{-\gamma t} K_t(g)\,\mathrm{d}t$, $g \in SE(2)$, is a time integrated probability kernel obtained from a scale space kernel $K_t : SE(2) \to \mathbb{R}^+$ (satisfying $K_{t_1} *_{SE(2)} K_{t_2} = K_{t_1+t_2}$) which we shall derive in section 3 and where U and V denote two initial distributions on $SE(2)$. Finally, χ in (10) is a monotonic, homogenous greyvalue transformation on orientation scores such as $\chi(U)(x, y, \theta) = F(\mathrm{Re}\{U(x, y, \theta)\})$, with $F : \mathbb{R} \to \mathbb{R}$ given by $F(I) = |I|^p \mathrm{sign}(I)$, for some $p > 1$. Here we do not put sources and sinks by hand as delta-distributions on $SE(2)$, [19], but we use invertible orientation scores instead. So in (10) we set $U = V = \mathcal{W}_\psi f$ and consider the operators $\mathcal{W}_\psi f \mapsto \Phi(\mathcal{W}_\psi f) := \tilde{\Phi}(\mathcal{W}_\psi f, \mathcal{W}_\psi f)$. The motivation for our choice (10) comes from basic probability theory which we explain next.

3 Scale Spaces on $SE(2)$ Based on Stochastic Processes

By the results of the previous section an operator on orientation scores must be left invariant. Therefor we consider left invariant scale spaces. The PDE's of these scale spaces are stochastic differential equations corresponding to left invariant stochastic processes for line enhancement/completion.

Just like an image can be interpreted as a distribution of greyvalue particles over space, the absolute value of an orientation score can be interpreted as a

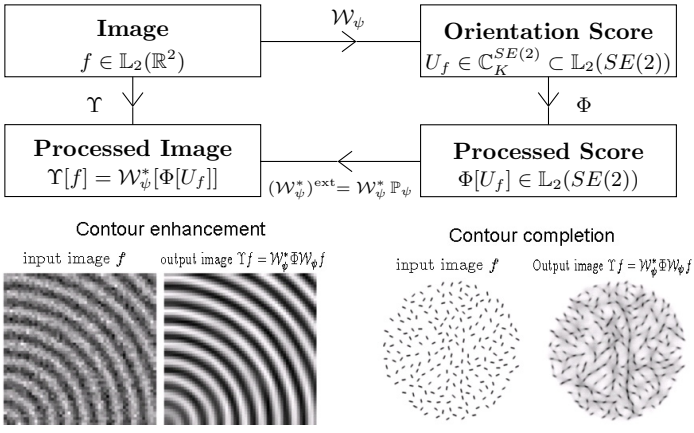

Fig. 1. The complete scheme; for admissible vectors ψ the linear map $\mathcal{W}_\psi$ is unitary from $\mathbb{L}_2(\mathbb{R}^2)$ onto the closed subspace of orientation scores $\mathbb{C}_K^{SE(2)}$ within $\mathbb{L}_2(SE(2))$. So we can uniquely relate an operator $\Phi : \mathbb{C}_K^{SE(2)} \to \mathbb{C}_K^{SE(2)}$ on an orientation score to an operator on an image $\Upsilon = (\mathcal{W}_\psi^*)^{ext} \circ \Phi \circ \mathcal{W}_\psi \in \mathcal{B}(\mathbb{L}_2(\mathbb{R}^d))$, where $(\mathcal{W}_\psi^*)^{ext}$ is given by (7) and where $\Phi(\mathcal{W}_\psi f) = \tilde{\Phi}(\mathcal{W}_\psi f, \mathcal{W}_\psi f)$ is given by (10) using the Green's functions/probability kernels $K_s := G_s^{D,\mathbf{a}} : SE(2) \to \mathbb{R}^+$ of the scale spaces (for line enhancement and completion) on $SE(2)$, that we shall derive in section 3.

distribution of *oriented* greyvalue particles over space and orientation. Next we derive suitable stochastic processes on this distribution of oriented greyvalue particles. We first consider a single oriented greyvalue particle with initial position $\mathbf{X}(0)$ and orientation $e^{i\Theta(0)}$ in $SE(2)$. We will apply superposition afterwards. For *line completion* this oriented greyvalue particle is send in the spatial plane along its preferred direction $\mathbf{e}_\xi = \cos\theta\,\mathbf{e}_x + \sin\theta\,\mathbf{e}_y$, $\xi = x\,\cos\theta + y\,\sin\theta$, allowing random behavior (with variance $\sigma^2 > 0$) of its orientation over time:

$$\begin{array}{l}(X_{n+1}, \Theta_{n+1}) := (X_n, \Theta_n) + \Delta s(\cos\Theta_n\,\mathbf{e}_x + \sin\Theta_n \mathbf{e}_y, \kappa_0) + \sqrt{\Delta s}\,\sigma\,\epsilon_{n+1}(0,0,1), \\ (X_0, \Theta_0) = (\mathbf{0}, 0), \text{ where } \epsilon_{n+1} \sim \mathcal{N}(0,1) \text{ independently normally distributed ,}\end{array} \tag{11}$$

with steps $\Delta s = L/N$, total length L of the trajectory, $n = 0, 1, \ldots, N-1$, $N \in \mathbb{N}$ and κ_0 an a priori curvature. This stochastic process is known in computer vision as the direction process [15], see Figure 2. By infinite repetition of this process one gets a limiting distribution $G : SE(2) \times \mathbb{R}^+ \to \mathbb{R}^+$ of greyvalue particles which (by Ito's formula) satisfies the following Fokker-Plank equation

$$\begin{array}{l}\partial_s G(x,y,\theta,s) = \left(-\partial_\xi - \kappa_0\,\partial_\theta + D_{11}(\partial_\theta)^2\right)\,G(x,y,\theta,s) \\ G(\cdot,\, s=0) = \delta_{g_0} = \delta_{x_0} \otimes \delta_{y_0} \otimes \delta_{\theta_0}\end{array} \tag{12}$$

In a Markov-process traveling time s is memoryless. Therefore s must be negatively exponentially distributed, i.e. $P(S = s) = \gamma e^{-\gamma s}$ with expectation $E(s) = \gamma^{-1}$. Now by superposition the probability densities of finding an oriented greyvalue particle at time $s > 0$, at position (x, y) with orientation θ, starting from the distribution $U \in \mathbb{L}_1(SE(2))$ at $s = 0$, equals

$$\begin{array}{l} P(x,y,\theta \mid U, S=s) = (G_s^{D_{11}} *_{SE(2)} U)(x,y,\theta) \text{ with } G_s^{D_{11}}(x,y,\theta) = G(x,y,\theta,s) \\ P(x,y,\theta \mid U) = \int_{\mathbb{R}^+} P(x,y,\theta \mid U, S=s) P(S=s) \mathrm{d}s = (R_s^{D_{11}} *_{SE(2)} U)(x,y,\theta)\ , \end{array} \tag{13}$$

where $P(S=s) = \gamma e^{-\gamma s}$ so that $R_\gamma^{D_{11}} = \gamma \int_0^\infty G_s^{D_{11}}\, e^{-\gamma\, s} \mathrm{d}s$. For *line enhancement*, we consider a different stochastic process on $SE(2)$:

$$\begin{array}{l} (X_{n+1}, \Theta_{n+1}) := (X_n, \Theta_n) + \sqrt{\Delta s}\, (\sigma_2 \epsilon_{n+1}^2 (\mathbf{e}_x \cos\Theta_n + \mathbf{e}_y \sin\Theta_n)\, ,\, \sigma_1\, \epsilon_{n+1}^1), \\ (X_0, \Theta_0) = (\mathbf{0}, 0), \text{ with } \epsilon_{n+1}^i \sim \mathcal{N}(0,1) \text{ independently normally distributed}\ , \end{array} \tag{14}$$

where $i = 1, 2$. Again by infinite concatenation of this process one gets a limiting distribution which satisfies following Fokker-Planck equation

$$\begin{array}{l} \partial_s G_{s,g_0}^{D_{11},D_{22}}(x,y,\theta) = \left(D_{11}(\partial_\theta)^2 + D_{22}(\partial_\xi)^2\right) G_{s,g_0}^{D_{11},D_{22}}(x,y,\theta) \\ G_{0,g_0}^{D_{11}}(\cdot) = \delta_{g_0} = \delta_{x_0} \otimes \delta_{y_0} \otimes \delta_{\theta_0}, \end{array} \tag{15}$$

with $\xi = x\cos\theta + y \sin\theta$, which coincides with Citti's model for perceptional enhancement in $SE(2)$, [3]. Next we consider all linear left invariant 2nd-order scale spaces on the Euclidean motion group $SE(2)$, whose solutions are $SE(2)$-convolutions with the corresponding Green's functions. In two particular cases we arrive at the Green's functions (12) and (15). In contrast to previous work [15] and [3], we provide the exact Green's functions.

3.1 Left-Invariant Scale Spaces on $SE(2)$

A vector field X on $SE(2)$ is called left invariant if for all $g \in SE(2)$ the push-forward of $(L_g)_* X_e$ by left multiplication $L_g h = hg$ equals X_g, that is

$$(X_g) = (L_g)_*(X_e) \Leftrightarrow X_g f = X_e(f \circ L_g), \text{ for all } f \in C^\infty : \Omega_g \to \mathbb{R}, \tag{16}$$

where Ω_g is some open set around $g \in SE(2)$. Recall that the tangent space at the unity element $e = (0,0,e^{i0})$ is spanned by $\{\mathbf{e}_x, \mathbf{e}_y, \mathbf{e}_\theta\} = \{(1,0,0),(0,1,0),(0,0,1)\}$ and by the general recipe explained in [5] we get the following basis for the space of left-invariant vector fields, $\mathcal{L}(\mathrm{SE}(2))$:

$$\begin{array}{l} \{\mathcal{A}_1, \mathcal{A}_2, \mathcal{A}_3\} := \{\partial_\theta, \partial_\xi, \partial_\eta\} = \{\partial_\theta, \cos\theta\, \partial_x + \sin\theta\, \partial_y, -\sin\theta\, \partial_x + \cos\theta\, \partial_y\}, \\ \text{with } \xi = x\, \cos\theta + y\, \sin\theta \text{ and } \eta = -x\, \sin\theta + y\, \cos\theta. \end{array} \tag{17}$$

Note that the non-commutative behavior of the group is intuitively reflected in a non-commuting Lie-algebra:

$$[\mathcal{A}_1, \mathcal{A}_2] = \mathcal{A}_1\mathcal{A}_2 - \mathcal{A}_2\mathcal{A}_1 = \mathcal{A}_3, \quad [\mathcal{A}_1, \mathcal{A}_3] = -\mathcal{A}_2, \quad [\mathcal{A}_2, \mathcal{A}_3] = 0\ .$$

Next we follow our general theory for left invariant scale spaces on Lie-groups, [5] and set the following quadratic form on $\mathcal{L}(SE(2))$, with $\mathbf{a} = (a_1, a_2, a_3) \in \mathbb{R}^3$,

$$Q^{\mathbf{D},\mathbf{a}}(\mathcal{A}_1, \mathcal{A}_2, \mathcal{A}_3) = \sum_{i=1}^3 \left(-a_i \mathcal{A}_i + \sum_{j=1}^3 D_{ij} \mathcal{A}_i \mathcal{A}_j \right),\ D := [D_{ij}] \in \mathbb{R}^{3\times 3}, \tag{18}$$

with $D^T = D \geq 0$ and consider the linear left-invariant scale spaces on $SE(2)$:

$$\begin{cases} \partial_s W(g,s) = Q^{\mathbf{D},\mathbf{a}}(\mathcal{A}_1,\mathcal{A}_2,\mathcal{A}_3)\, W(g,s)\ , & s>0, g \in SE(2). \\ W(g,s=0) = U(g)\ , & g \in SE(2). \end{cases} \tag{19}$$

with corresponding resolvent equations (obtained by Laplace transform over s):

$$P_\gamma(g) = \gamma(Q^{\mathbf{D},\mathbf{a}}(\mathcal{A}_1,\mathcal{A}_2,\mathcal{A}_3) - \gamma I)^{-1} U(g) \tag{20}$$

which (for the cases $\mathbf{a} = \mathbf{0}$) correspond to first order Tikhonov regularization on $SE(2)$, [5]. By our results in [5], the solutions of these left invariant evolution equations are $SE(2)$-convolutions with the corresponding Green's function:

$$W(\mathbf{x},\theta,s) = (G_s^{\mathbf{D},\mathbf{a}} *_{SE(2)} U)(\mathbf{x},\theta), \qquad P_\gamma(\mathbf{x},\theta) = (R_\gamma^{\mathbf{D},\mathbf{a}} *_{SE(2)} U)(\mathbf{x},\theta)$$

where we recall (9). In the special case $D_{ij} = \frac{1}{2}\sigma^2\delta_{i1}\delta_{j1}$, $i,j = 1,2,3$, and $\mathbf{a} = (\kappa_0, 1, 0)$ our scale space equation (19) is the Fokker-Planck equation (12) of Mumford's direction process for line completion and in the case $D_{ij} = D_{ii}\delta_{ij}$, $D_{11} = \frac{1}{2}(\sigma_1)^2$, $D_{22} = \frac{1}{2}(\sigma_2)^2$, $D_{33} = 0$, $\mathbf{a} = \mathbf{0}$, our scale space equation is the Fokker-Planck equation (15) of the stochastic process for line enhancement. Next we provide the exact Green's functions with suitable approximations, but first we provide a simple intuitive, but nevertheless analogous, example.

3.2 A Simple Introductory Example: Scale Spaces on the Circle

The Gaussian scale space equation and corresponding resolvent equation on a circle $\mathbb{T} = \{e^{i\theta} \mid \theta \in [0, 2\pi)\}$ with group product $e^{i\theta}e^{i\theta'} = e^{i(\theta+\theta')}$, read

$$\begin{cases} \partial_s u(\theta,s) = D_{11}\partial_\theta^2 u(\theta,s), \\ u(0,s) = u(2\pi,s) \text{ and } u(\theta,0) = f(\theta) \end{cases} \text{ and } p_\gamma(\theta) = \gamma(D_{11}\partial_\theta^2 - \gamma I)^{-1} f(\theta), \tag{21}$$

with $\theta \in [0, 2\pi)$ and $D_{11} > 0$ fixed, where we recall that the function $\theta \mapsto p_\gamma(\theta) = \gamma \int_0^\infty u(\theta,s)e^{-\gamma s}\mathrm{d}s$ is the minimizer of the energy

$$\mathcal{E}(p_\gamma) := \int_0^{2\pi} \gamma |p_\gamma(\theta) - f(\theta)|^2 + D_{11}|p_\gamma'(\theta)|^2 \mathrm{d}\theta$$

under the periodicity condition $p_\gamma(0) = p_\gamma(2\pi)$. By left-invariance the solutions are given by $\mathbb{T}$-convolution with their Green's function (or "impuls-response"), say $G_s^{D_{11}} : \mathbb{T} \to \mathbb{R}^+$ and $R_\gamma^{D_{11}} : \mathbb{T} \to \mathbb{R}^+$. Note that $R_\gamma^{D_{11}} = \gamma \int_0^\infty G_s^{D_{11}} e^{-\gamma s}\mathrm{d}s$. Now orthogonal eigenfunctions of the diffusion process correspond to eigenfunctions of the generator $D_{11}(\partial_\theta)^2$ and they are given by $\eta_n(\theta) = \frac{e^{in\theta}}{\sqrt{2\pi}}$, so that

$$\begin{aligned} u(\theta,s) &= \sum_{n\in\mathbb{Z}} (\eta_n, f)_{\mathbb{L}_2(\mathbb{T})} \eta_n(\theta) e^{-n^2 s D_{11}} \ , \quad G_s^{D_{11}}(\theta,s) = \sum_{n\in\mathbb{Z}} \eta_n(\theta)\eta_n(0) e^{-n^2 s D_{11}} \ , \\ p_\gamma(\theta) &= \sum_{n\in\mathbb{Z}} (\eta_n, f)_{\mathbb{L}_2(\mathbb{T})} \eta_n(\theta) \tfrac{\gamma}{D_{11}n^2+\gamma} \ , \quad R_\gamma^{D_{11}}(\theta) = \sum_{n\in\mathbb{Z}} \eta_n(\theta)\eta_n(0) \tfrac{\gamma}{D_{11}n^2+\gamma} \ . \end{aligned} \tag{22}$$

A well-known drawback of such an approach is that the series do not converge quickly if $s > 0$ resp. $\gamma > 0$ are small. In such case one of course prefers a spatial

implementation over a Fourier implementation, where one unfolds the circle and calculate modulo 2π-shifts afterwards, i.e.

$$u(\theta,s) = (G_s^{D_{11}} * f)(\theta)\ ,\ \text{where } G_s^{D_{11}}(\theta) = \sum_{n\in\mathbb{Z}} G_s^{D_{11},\infty}(\theta - 2\pi n) \tag{23}$$

where the Green's functions for diffusion and Tikhonov regularization on $\mathbb{R}$ are $G_s^{D_{11},\infty}(\theta) = (4\pi s)^{-1/2} e^{-\frac{\theta^2}{4s}}$ and $R_\gamma^{D_{11},\infty}(\theta) = \gamma \int_{\mathbb{R}^+} G_s^{D_{11},\infty} e^{-\gamma s} \mathrm{d}s = \frac{\gamma}{2} e^{-\sqrt{\gamma}|\theta|}$. Again the latter formula follows by Laplace transform of the first, but a better derivation is by means of a continuous (not differentiable) fit at θ of two solutions in the nullspace of operator $(\partial_\theta^2 + \gamma)$ which vanish resp. at $+\infty$ and $-\infty$. The sums in (23) can be computed explicitly, yielding $G_s^{D_{11}}(\theta) = \frac{1}{2\pi}\vartheta_3\left(\frac{\theta}{2\sqrt{D_{11}}}, e^{-s}\right)$, where ϑ_3 is a theta-function of the 3rd kind.

3.3 The Green's Functions of the Line-Completion Process

Let us consider the case $D_{ij} = \frac{\sigma^2}{2}\delta_{i1}\delta_{j1}$, $\mathbf{a} = (\kappa_0, 1, 0)$ where our scale space equation (19) equals the Fokker-Planck equation (12) of Mumford's direction process. The next theorems provide formulas (like (22)) for the Green's function in terms of Mathieu-functions, using the conventions as in cf. [14], $\mathrm{me}_\nu(z,q)$, $\mathrm{ce}_\nu(z,q)$ with Floquet exponent ν, such that $\mathrm{Im}(\nu) \geq 0$.

Theorem 1. *The Green's functions $R_\gamma^{D_{11}}, G_s^{D_{11}} \in C^\infty(SE(2)\setminus\{e\})$, of the direction process with $\kappa_0 = 0$, i.e. the unique smooth solutions of*

$$\begin{cases} \left(\partial_\xi - D_{11}\partial_\theta^2 + \gamma\right) R_\gamma^{D_{11}} = \gamma\,\delta_e, \\ R_\gamma^{D_{11}}(\cdot,0) = R_\gamma^{D_{11}}(\cdot,2\pi) \end{cases} \quad \begin{cases} \partial_s G_s^{D_{11}} = \left(-\partial_\xi + D_{11}\partial_\theta^2\right) G_s^{D_{11}} \\ G_s^{D_{11}}(\cdot,0) = G_s^{D_{11}}(\cdot,2\pi), \lim_{s\downarrow 0} G_s^{D_{11}} = \delta_e \end{cases} \tag{24}$$

$$\begin{aligned} &\text{are } R_\gamma^{D_{11}}(x,y,\theta) = \mathcal{F}^{-1}\left(\boldsymbol{\omega} \mapsto \sum_{n=0}^{\infty} \frac{\gamma}{\pi^2 \lambda_n(\rho)} ce_n\left(\tfrac{-\varphi}{2}, i\tfrac{2\rho}{D_{11}}\right) ce_n\left(\tfrac{\theta-\varphi}{2}, i\tfrac{2\rho}{D_{11}}\right)\right)(x,y), \\ &G_s^{D_{11}}(x,y,\theta) = \mathcal{F}^{-1}\left(\boldsymbol{\omega} \mapsto \sum_{n=0}^{\infty} \frac{e^{-\frac{a_n^2(\rho)s}{D_{11}}}}{\pi^2} ce_n\left(\tfrac{-\varphi}{2}, i\tfrac{2\rho}{D_{11}}\right) ce_n\left(\tfrac{\theta-\varphi}{2}, i\tfrac{2\rho}{D_{11}}\right)\right)(x,y) \end{aligned} \tag{25}$$

with $\boldsymbol{\omega} = (\rho\cos\varphi, \rho\sin\varphi)$, $-\lambda_n(\rho) = -a_n(\frac{2i\rho}{D_{11}}) - \gamma < 0$, where $a_n(h^2)$ denote the positive eigenvalues of Mathieu's equation, cf. [14]. The Green's function $R_\gamma^{D_{11}}$ is indeed a probability kernel, i.e. $R_\gamma^{D_{11}} > 0$ and $\int_{SE(2)} R_\gamma^{D_{11}}(g)\mathrm{d}g = 1$.

For detailed proof we refer to our latest work [7], where our most relevant observation is that the generator $B = -\partial_\xi + D_{11}\partial_\theta^2$ of the line-completion process in the Fourier domain (only with respect to (x,y)) reads

$$\hat{B} = \mathcal{F}B\mathcal{F}^{-1} = -i\omega_x\cos\theta - i\omega_y\sin\theta + D_{11}\partial_\theta^2 = -i\rho\cos(\theta-\varphi) + D_{11}\partial_\theta^2, \tag{26}$$

so (25) is a bi-orthogonal expansion of eigen functions (directly related to the Mathieu functions, which are eigen functions of $\partial_z^2 - 2h^2\cos(2z)$) of the restriction of $-\hat{B} + \gamma I$ to the circle $\mathbb{T}$. The formulae (25) are the exact solutions of the numerical algorithm by August [1]. The drawback, however, of this bi-orthogonal

expansion is the speed of convergence near e. This inspired us to find a much better series representation: The idea here is to make a continuous (but not differentiable at $\theta = 0$!) fit of elements on each side of the singularity at $\theta = 0$ within the nil-space of $-\hat{B}+\gamma I$ that vanish at $\theta \to \pm\infty$. Here we unfold the circle providing a series of 2π-shifts of the solutions with infinite boundary conditions. For relevant parameter settings this series can be truncated at $N=0,1$ or at the most $N=2$ if D_{11}/γ is small. This yields the following analogue of (23):

Theorem 2. *The Green's function $R_\gamma^{D_{11}}$ of the direction process with a priori curvature $\kappa_0 \geq 0$, i.e. the unique smooth solution of (24), is given by*

$$R_\gamma^{D_{11}}(\boldsymbol{x},\theta) = \mathcal{F}^{-1}(\boldsymbol{\omega} \mapsto \hat{R}_\gamma^{D_{11}}(\boldsymbol{\omega},\theta))(\boldsymbol{x}),$$

with $\hat{R}_\gamma^{D_{11}}(\boldsymbol{\omega},\theta) = \lim_{N\to\infty} \sum_{k=-N}^{N} \hat{R}_{\gamma,\infty}^{D_{11}}(\boldsymbol{\omega},\theta-2k\pi)$, where the Fourier transform $\hat{R}_{\gamma,\infty}^{D_{11}} = \mathcal{F}R_{\gamma,\infty}^{D_{11}}$ of the solution $R_{\gamma,\infty}^{D_{11}}$ of

$$\begin{cases} \left(\partial_\xi - D_{11}(\partial_\theta)^2 + \gamma\right) R_\gamma^{D_{11},\infty} = \gamma\delta_e \\ R_\gamma^{D_{11},\infty}(\cdot,\theta) \to 0 \text{ uniformly on compacta as } |\theta| \to \infty \end{cases}$$

is given by $\hat{R}_{\gamma,\infty}^{D_{11}}(\omega_x,\omega_y,\theta) = \frac{-\gamma e^{\frac{\kappa_0\theta}{2D_{11}}}}{\pi D_{11} W(\rho)} \Big[me_\nu\left(\frac{\varphi}{2}, i\frac{2\rho}{D_{11}}\right) me_{-\nu}\left(\frac{\varphi-\theta}{2}, i\frac{2\rho}{D_{11}}\right) \mathrm{u}(\theta) + me_{-\nu}\left(\frac{\varphi}{2}, i\frac{2\rho}{D_{11}}\right) me_\nu\left(\frac{\varphi-\theta}{2}, i\frac{2\rho}{D_{11}}\right) \mathrm{u}(-\theta)\Big]$,
with Floquet exponent given by $\nu = \nu\left(\frac{-4\gamma}{D_{11}} - \frac{\kappa_0^2}{D_{11}^2}, \frac{2i\rho}{D_{11}}\right)$, *unitstep function* $\mathrm{u}(\theta) = \frac{1}{2}(1+sign(\theta))$, *and the function $W(\rho)$ denotes the Wronskian of $me_\nu(\cdot, i\frac{2\rho}{D_{11}})$ and $me_{-\nu}(\cdot, i\frac{2\rho}{D_{11}})$.*

Remark. The sum in Theorem 2 can be computed explicitly (by Floquet's theorem) yielding a single exact formula on $SE(2)$ consisting of only 4 Mathieu functions [18, p.127], [7, ch:4.2.1], likewise the ϑ-function of subsection 3.2. However it still requires sampling of Mathieu-functions, therefore we derive a parametrix (see [3], [17]) by replacing the true left invariant vector fields $\{\mathcal{A}_1,\mathcal{A}_2,\mathcal{A}_3\}$ on $SE(2)$ by

$$\{\hat{A}_1,\hat{A}_2,\hat{A}_3\} = \{\partial_\theta, \partial_x + \theta\partial_y, -\theta\partial_x + \partial_y\}. \tag{27}$$

Essentially, this replaces the group of positions and orientations, locally by the (nilpotent) group of positions and velocities (normalized in x-direction). See Figure 2. By some theory on nilpotent Lie groups it follows, see [4]p.166, that

$$\tilde{G}_s^{D_{11}}(x,y,\theta) = \frac{\sqrt{3}}{2\,D_{11}\pi x^2}\,\delta(x-s)\,e^{-\frac{3(x\theta-2y)^2+x^2(\theta-\kappa_0 x)^2}{4x^3 D_{11}}}, \tag{28}$$

yielding $\tilde{R}_\gamma^{D_{11}}(x,y,\theta) = \frac{\gamma\sqrt{3}\,e^{-\frac{3(x\theta-2y)^2+x^2(\theta-\kappa_0 x)^2-\gamma x}{4x^3 D_{11}}}}{2\,D_{11}\pi x^2}\mathrm{u(x)}$ by Laplace transform.

3.4 The Green's Functions of the Line-Enhancement Process

In this paragraph we will derive the Green's functions of the line-enhancement process (14). These kernels are the exact heat-kernels for a Gaussian scale space

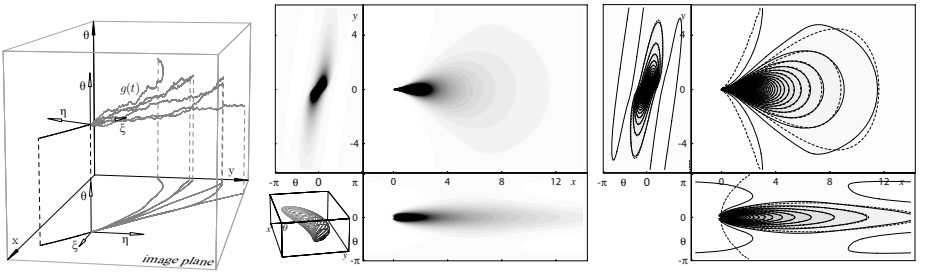

Fig. 2. Left: Random walks of the direction process (11). Middle: isoline-plots of the marginals of $R_\gamma^{D_{11}}$, which is the time-integrated limiting distribution (using Ito-calculus) of all random walks, $\gamma = \frac{1}{10}$, $D_{11} = \frac{1}{32}$, $\kappa_0 = 0$. Left corner middle image: 3D-plot of 2D-isolines of $R_\gamma^{D_{11}}$. Right: a comparison of the level curves of the marginals of $\tilde{R}_\gamma^{D_{11}}$ and $R_\gamma^{D_{11}}$. Dashed lines denote the level sets of approximation $\tilde{R}_\gamma^{D_{11}}$, see (28).

on the group of positions and orientations. Here we even allow $D_{33} \geq 0$. Set $D_{33} = 0$ to get the Green's functions of (14).

Theorem 3. *Let $D_{11}, D_{22}, D_{33} > 0$, then the Green's function (or rather Gaussian kernels) $G_s^{D_{11},D_{22},D_{33}}$ on the Euclidean motion group $SE(2)$ of the scale space equation (19) generated by (18) with $\boldsymbol{a} = \boldsymbol{0}$ and $D_{ij} = D_{ii}\delta_{ij}$ is given by*

$$G_s^{D_{11},D_{22},D_{33}}(b_1, b_2, e^{i\theta}) = \mathcal{F}^{-1}[\boldsymbol{\omega} \mapsto \hat{G}_s^{D_{11},D_{22},D_{33}}(\boldsymbol{\omega}, e^{i\theta})](b_1, b_2), \text{ with}$$

$$\hat{G}_s^{D_{11},D_{22},D_{33}}(\boldsymbol{\omega}, e^{i\theta}) = \frac{e^{-s(1/2)(D_{22}+D_{33})\rho^2}}{\pi}\left(\sum_{n=0}^{\infty} ce_n(\varphi, q)\, ce_n(\varphi-\theta, q) e^{-s\, a_n(q) D_{11}}\right)$$

with $q = q(\rho) = \frac{\rho^2(D_{22}-D_{33})}{4\,D_{11}}$ and $a_n(q)$ the Mathieu Characteristic. For relatively simple formula for the corresponding resolvent Green's functions $R_{\gamma,\infty}^{D_{11},D_{22},D_{33}}$ analogous to the formulas in Theorem 2 see [6, part I, Thm 5.2, 5.3].

For $D_{33} < D_{22}$ the resolvent (or Tikhonov regularization) kernel on $SE(2)$ $R_\gamma^{D=diag\{D_{11},D_{22},D_{33}\}}$ is given by

$$\begin{aligned}
&[\mathcal{F}R_\gamma^D(\cdot,\theta)](\omega) = \tfrac{\gamma}{4\pi D_{11}\, ce_\nu(0,q)\, se'_\nu(0,q)}\,\{\\
&(-\cot(\nu\pi)\,(ce_\nu(\varphi,q)\, se_\nu(\varphi-\theta,q) + se_\nu(\varphi,q)\, se_\nu(\varphi-\theta,q)) +\\
&\quad ce_\nu(\varphi,q)\, se_\nu(\varphi-\theta,q) - se_\nu(\varphi,q)\, ce_\nu(\varphi-\theta,q))\,\mathrm{u}(\theta) \quad +\\
&(-\cot(\nu\pi)\,(ce_\nu(\varphi,q)\, ce_\nu(\varphi-\theta,q) - se_\nu(\varphi,q)\, se_\nu(\varphi-\theta,q)) +\\
&\quad ce_\nu(\varphi,q)\, se_\nu(\varphi-\theta,q) + se_\nu(\varphi,q)\, ce_\nu(\varphi-\theta,q))\,\mathrm{u}(-\theta)\quad \},
\end{aligned} \tag{29}$$

with $q = \frac{(D_{22}-D_{33})\rho^2}{4D_{11}}$, $\omega = (\rho\cos\varphi, \rho\sin\varphi)$, Floquet exponent $\nu = \nu(a,q)$ and $a = -\frac{\gamma+(1/2)(D_{22}-D_{33})\rho^2}{D_{11}}$.

For the corresponding Green's functions on the group of positions and velocities, recall (27), see [5]. Finally, in [6, ch:5.4] we derive the useful formula:

$$\begin{aligned}
&K_s^{D_{11},D_{22}}(x, y, e^{i\theta}) \approx\\
&\frac{1}{4\pi s^2 D_{11} D_{22}} e^{-\frac{1}{4s\,c^2}\sqrt{\left(\frac{\theta^2}{D_{11}} + \frac{\theta^2(y-\eta)^2}{4(1-\cos(\theta))^2 D_{22}}\right)^2 + \frac{1}{D_{11}D_{22}}\left(\frac{\theta^2(\xi-x)^2}{4(1-\cos\theta)^2}\right)}},
\end{aligned} \tag{30}$$

where we recall (17).

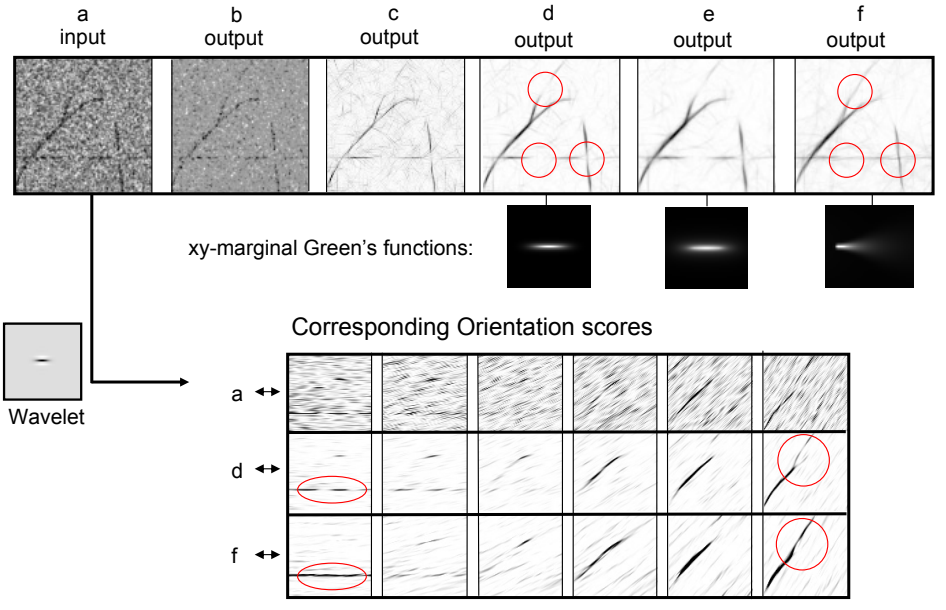

Fig. 3. Top row: a: noisy input image f, b: $|f|^p \text{sign} f$, c: $(\mathcal{W}_\psi^*)^{ext}(\chi_p(\mathcal{W}_\psi f))$ with $p = 1.5$, d,e: line enhancement using time-dependent diffusion kernel depicted below, f: line completion using resolvent completion-kernel depicted below. All involved orientation scores are sampled on a $100 \times 100 \times 64$ grid. Circles depict parts where a clear difference arises between line completion and enhancement. Middle row: proper wavelet ψ in example of section 2 (par's $k = 2, n_\theta = 64$), Green's function line enhancement process par's $D_{11} = 0.00015$, $D_{22} = 1$, $s = 15$, using asymptotic formula (30), Green's function line enhancement process $D_{11} = 0.00015$, $D_{33} = 1$, $\gamma = \frac{1}{64}$, Green's function line completion process $D_{11} = 0.0024$, $\gamma = \frac{1}{64}$. Bottom row: Slices $\mathcal{W}_\psi f(\cdot, \cdot, e^{i\theta_k})$ for $\theta_k = (2k+1)\frac{\pi}{32}$, $k = 0, \ldots, 5$.

Now that we have derived the Green's functions we return to our scheme, Fig. 1. First, we construct an invertible orientation score (1). Then we convolve the orientation score with 2 Green's functions to compute the direct product in (10) and finally we apply the inverse transform (6). For experiments, see Fig. 3.

4 Conclusion

Since the transformations between image and orientation score are stable, we can apply image processing via orientation scores. To ensure Euclidean invariance of the operator on an image the corresponding operator on its orientation score must be left-invariant. Therefore we consider left-invariant scale spaces on these orientation scores based on stochastic processes on the group $SE(2)$, the solutions of which are given by $SE(2)$-convolution with the corresponding Green's functions, which we derived explicitly.

References

1. August, J.: The Curve Indicator Random Field. PhD thesis, Yale University (2001)
2. Candes, F.: New ties between computational harmonic analysis and approximation theory. Approximation Theory X, Innov. Appl. Math. (6), 87–153 (2000)
3. Citti, G., Sarti, A.: A cortical based model of perceptual completion in the roto-translation space. JMIV 24(3), 307–326 (2006)
4. Duits, R.: Perceptual Organization in Image Analysis. PhD thesis, Eindhoven University of Technology, Dep. of Biomedical Engineering, The Netherlands (2005)
5. Duits, R., Burgeth, B.: Scale spaces on lie groups. In: Sgallari, F., Murli, A., Paragios, N. (eds.) SSVM 2007. LNCS, vol. 4485, pp. 300–312. Springer, Heidelberg (2007)
6. Duits, R., Franken, E.M.: Left-invariant parabolic evolutions on $SE(2)$ and contour enhancement via invertible orientation scores, part i: Linear left-invariant diffusion equations on $SE(2)$. Quarterly of Appl. Math. (to appear, 2009)
7. Duits, R., van Almsick, M.A.: The explicit solutions of linear left-invariant second order stochastic evolution equations on the 2d-euclidean motion group. Quarterly of Applied Mathematics 66, 27–67 (2008)
8. Franken, E., Duits, R., ter Haar Romeny, B.M.: Nonlinear diffusion on the 2D euclidean motion group. In: Sgallari, F., Murli, A., Paragios, N. (eds.) SSVM 2007. LNCS, vol. 4485, pp. 461–472. Springer, Heidelberg (2007)
9. Franken, E.M.: Enhancement of Crossing Elongated Structures in Images. PhD thesis, Dep. of Biomedical Engineering, Eindhoven University of Technology, The Netherlands, Eindhoven (October 2008)
10. Grossmann, A., Morlet, J., Paul, T.: Integral transforms associated to square integrable representations. J. Math. Phys. 26, 2473–2479 (1985)
11. Kalitzin, S.N., ter Haar Romeny, B.M., Viergever, M.A.: Invertible apertured orientation filters in image analysis. IJCV 31(2/3), 145–158 (1999)
12. Louis, A.K., Maass, P., Rieder, P.: Wavelets, Theory and Applications. Wiley, New York (1997)
13. Medioni, G., Lee, M.S., Tang, C.K.: A Computational Framework for Segmentation and Grouping. Elsevier, Amsterdam
14. Meixner, J., Schaefke, F.W.: Mathieusche Funktionen und Sphaeroidfunktionen. Springer, Heidelberg (1954)
15. Mumford, D.: Elastica and computer vision. Algebraic Geometry and Its Applications, pp. 491–506. Springer, Heidelberg (1994)
16. Sporring, J., Nielsen, M., Florack, L.M.J., Johansen, P.: Gaussian Scale-Space Theory. KAP, Dordrecht (1997)
17. Thornber, K.K., Williams, L.R.: Analytic solution of stochastic completion fields. Biological Cybernetics 75, 141–151 (1996)
18. van Almsick, M.A.: Context Models of Lines and Contours. PhD thesis, Eindhoven University of Technology, Department of Biomedical Engineering, Eindhoven, The Netherlands (2007) ISBN:978-90-386-1117-4
19. Zweck, J., Williams, L.R.: Euclidean group invariant computation of stochastic completion fields using shiftable-twistable functions. JMIV 21(2), 135–154 (2004)